PCCP

ROYAL SOCIETY OF CHEMISTRY

PAPER

View Article Online
View Journal | View Issue

Cite this: *Phys. Chem. Chem. Phys.*, 2023, **25**, 9482

Effects of layer-by-layer coating on activated carbon electrodes for capacitive deionization

Sergio Orozco-Barrera, Guillermo R. Iglesias, Ángel V. Delgado, Sergio García-Larios and Silvia Ahualli *

Recently, the need for obtaining, reusing, or purifying water has become a crucial issue. The capacitive deionization (CDI) method, which is based on the electric double layer (EDL) concept, can be applied to ion adsorption from an aqueous solution. This process is carried out by applying a potential difference to highly porous electrodes while pumping salty solution between them, partially removing the ions present in the solution and keeping them in the surface of the electrodes. The use of coated carbon electrodes with one polyelectrolyte layer, turning them into "soft electrodes" (SEs), has been proved to improve the efficiency of the system with respect to its original configuration. In this work, we investigate the effect on the ion adsorption and the efficiency of the process when implementing the coating technique known as layer-by-layer (LbL) on the electrode. This consists in successively coating the electrode surfaces with polyelectrolyte layers, alternating their charge polarity in each step. We tested the effect of the number of layers deposited, as well as the impact of this technique by using different carbons. We found that the second polyelectrolyte layer adheres more than the first layer, serving as a support or seed when it is not dense and uniformly distributed. In contrast, if the first layer is well adhered, a third layer is needed to observe improvements in adsorption and process efficiency. The adsorption of the polymer layers depends in any instance on the porosity of the carbon.

Received 7th December 2022,
Accepted 21st February 2023

DOI: 10.1039/d2cp05682h

rsc.li/pccp

1. Introduction

Methods for non-consumable-water treatment have been studied for years now. Following this line, and based on the "electrochemical demineralization of water" proposed by Blair, Murphy *et al.*[1] capacitive deionization (CDI) emerges as a renewable alternative to traditional methods[2] at a functional level with low energetic costs. This technique is based on electric double layer (EDL) properties[3,4] to partially remove ions from a saline solution being pumped between a couple of highly porous electrodes facing each other when applying a potential difference between them. With the application of this potential difference, ions migrate to their oppositely charged electrode, contributing to the EDL formation on the interface until the electrode surface charge is completely screened. The EDL has the typical storage properties of a capacitor, and its capacitance will be higher the larger the usable interfacial area between the solution and the electrode. It is then necessary to use materials such as activated carbon for the electrode surface, due to its high conductivity and specific surface area (high porosity): its large number of pores act as microscopic channels for ion storage. This desalination process has been found to be optimum when desalinating solutions up to 10 g L^{-1}.

In the search for an improvement of this method, promising results in desalination have been found by coating the carbon electrodes with polyelectrolyte (PE) layers, turning them into so-called "soft electrodes" (SE). These PE layers are chosen to have a positive (negative) charge density when adhered to the positively (negatively) charged electrode surface, favoring the counterion transport and blocking the coion one from entering or exiting the EDL.[5,6] This method is similar to "membrane assisted-CDI" (MCDI)[7–9] although with a lower overall performance, but with the advantage of a lower economic cost and ease of preparation. Furthermore, considering that the PE coating does not add to the system a higher internal resistance, setting up this technique is a more than plausible approach.

One of the reasons why SE has a lower performance than MCDI is that the polymer charge density is small compared to that of an ion exchange membrane. Besides, the coating is not uniform in the sense that not all the surface of the macropores is lined with the polymer. For that reason, in the present work, the use of SEs has been approached with the application of PE multilayers and the consideration of its impact on ion transport and adsorption. This multiple coating technique is known as Layer-by-Layer (LbL),[10] widely used due to its simple application:[11,12] PE layers are successively deposited onto the desired

Department of Applied Physics, Faculty of Science, University of Granada, 18071 Granada, Spain. E-mail: sahualli@ugr.es

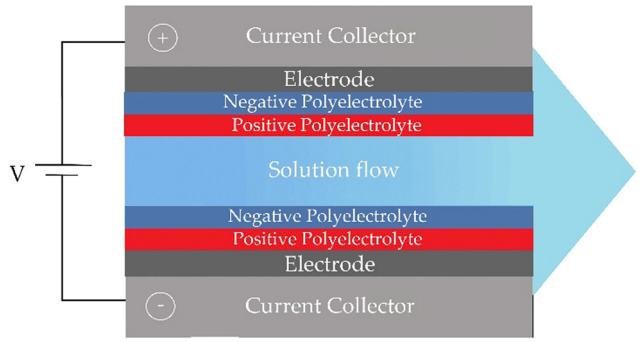

Fig. 1 Scheme of the electrodes coated with two polyelectrolyte layers.

surface while alternating their charge polarity. This work has been experimentally addressed to prepare these LbL-coated carbon electrodes for CDI use (a scheme of the LbL-electrodes is shown in Fig. 1). On the other hand, a theoretical model has been proposed to bring light to the ion transport behavior while using these electrode configurations with multiple PE layers. The coating is strongly dependent on the size and porosity of the macropores, which is where the PE chains are deposited. Two different activated carbons have been used as a base of the electrodes, in order to study possible differences in coating and adherence of the PE layers depending on the characteristics of the carbon used, such as its specific surface area, electrical resistance, and porosity.

2. Experimental

2.1. Materials

For the experimental work, 10 mM NaCl (Sigma-Aldrich, Darmstadt, Germany) solutions were prepared. The water used was previously deionized and filtered with a Milli-Q Academic System (Millipore, Molsheim, France).

The carbon particles employed for the preparation of the electrodes were SR23 (MAST Carbon International Ltd, UK) and YP-80F (Kuraray Co. Ltd, Japan), which are ideal for this work due to their huge available surface area (S_{SR23} = 959 m^2 g^{-1}; $S_{YP\text{-}80F}$ = 2271 m^2 g^{-1}) for ion adsorption and storage. The pore size distribution is 7 nm for the SR23 carbon,[13] and 1 nm for the YP-80F as specified by the manufacturer. Black carbon (Alfa Aesar, Termo Fisher, Germany) has also been used in small quantities to boost the electrical conductivity of the electrodes.[14]

In order to prepare the polyelectrolyte coatings, aqueous solutions of poly(diallyldimethyl-ammonium chloride) (PDADMAC, with a molecular weight of 200 000 g mol^{-1}, cationic) and poly(sodium 4-styrenesulfonate) (PSS, molecular weight of 100 000 g mol^{-1}, anionic) were prepared. Both polymers were purchased from Sigma-Aldrich.

2.2. Setup

The experimental setup was based on two planar electrodes, facing each other at a distance of 500 μm by a nylon spacer. Each of these electrodes was formed by a 10 cm long and 5 cm wide graphite plate used as a current collector, onto which the activated carbon was deposited (see Fig. 2). The carbon on the electrode was previously prepared as a mixture of the given activated carbon powder and black carbon (5% black carbon; 95% activated carbon), and a 33 g L^{-1} solution of poly(vinylidene-fluoride) (PVDF, manufactured by Arkema, Colombes, France, as Kynar HSV 900, with a molecular weight of approximately 1 000 000) in 1-methyl 2-pyrrolidone (Sigma Aldrich). For the SR23 activated carbon, 3 g of the SR23 + black carbon were mixed with 10 g of PVDF. In the case of YP-80F activated carbon, 3 g of the YP-80F + black carbon and 12 g of PVDF were mixed. The final carbon suspension was deposited onto the graphite collector as a 500 μm layer using the doctor blade technique, and dried at 60 °C for 24 h.

The polymeric coating of the electrodes was carried out by immersing them in a 200 mM aqueous solution of the corresponding polyelectrolyte (PDADMAC for the positive electrode, PSS for the negative electrode) for 6 h under constant magnetic

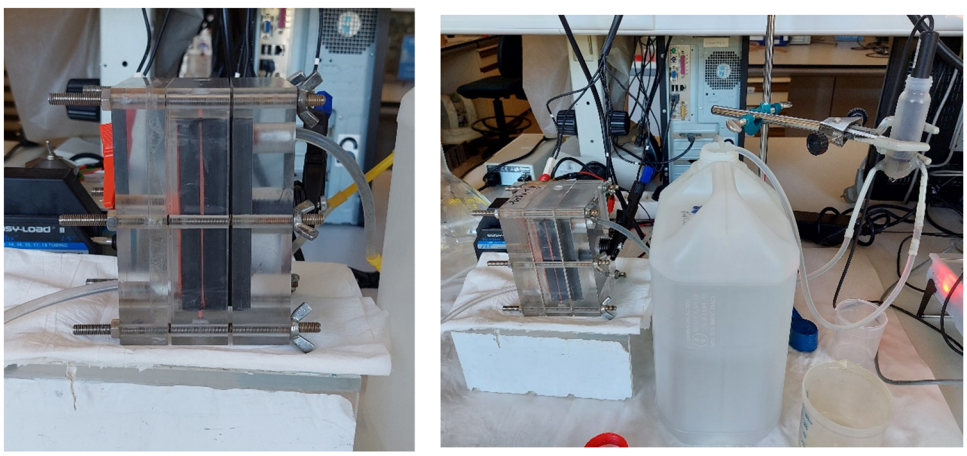

Fig. 2 Left: Picture of the working cell, where the planar electrodes facing each other can be observed. At the lower left side of the cell, the solution inlet can be appreciated, as well as the outlet at the upper right side of the cell. Right: Photography of the complete circuit at work. The solution is pumped from the vessel to the cell, and the outlet solution is measured with the probe, which can be seen at the upper right side.

stirring. In order to carry out the Layer-by-Layer process, both electrodes were immersed alternately into the polyelectrolyte solution with opposite charge density, favoring its adherence *via* electrostatic interactions. Electrophoretic mobilities were measured in each step in order to check whether the coating was done correctly. In addition, diameters of 400 ± 120 nm for the YP-80F bare carbon particles compared to diameters of 640 ± 130 nm and 460 ± 100 nm for the PDADMAC-coated and PSS-coated ones, respectively, show a slight increase due to the coatings. Note that the uncertainty in the measurements comes from the polydispersity of the carbon particles.

Once the electrodes were prepared, the measurement cell was set up as described above. The desalination process took place by pumping the saline solution through the cell from a 5 L container. The cell is connected to an Iviumstat.h (Ivium, The Netherlands) potentiostat working at constant voltage. Changes in conductivity and temperature were measured at the exit of the cell with a 529670 probe (Leybold, Dresden, Germany) and continuously read by a Leybold 524D10 Cassy Lab interface. The exit solution was returned to the original container, which was large enough to keep the inlet conductivity appreciably constant during successive working cycles (Fig. 2).

Each CDI cycle involves two steps: in the adsorption one, the electrodes are powered by applying a constant voltage (1.2 V) from the source, which drives ions from the solution flow to the macropores of the electrode with opposite charge, decreasing the measured conductivity. During the desorption step, the stored ions are released to the main solution flow, allowing the carbon pores to become empty for the following adsorption step. Desorption was carried out by externally short-circuiting the electrodes (Zero-Voltage, ZV, condition), draining the pores, and returning the ions to the solution, which was detected as an increase in the on-line conductivity sensor.

From the conductivity values, the concentration difference is calculated *via* the relationship:

$$K = \frac{N_A e^2 c (D_{Na} + D_{Cl})}{k_B T} \quad (1)$$

where K is the conductivity, c is the common ion concentration in the solution, and D_{Na} and D_{Cl} are the diffusion coefficients of the ions (1.33×10^{-9} m^2 s^{-1} for Na^+ and 2.03×10^{-9} m^2 s^{-1} for Cl^-). T is the system temperature, k_B is the Boltzmann constant, and N_A is the Avogadro number.

3. Results and discussion

3.1. SR23 carbon electrodes

3.1.1. Bare carbon electrodes and soft electrodes: first layer effect. As described above, removing ions from the solution translates into a decrease in the conductivity until the charge on the electrodes is screened by the EDL. Since the solution is constantly pumped in these experiences, the conductivity returns to the feed solution value after reaching its minimum value. Hence, the larger the area under the curve conductivity/concentration difference *vs.* time in the adsorption stage, the larger the number of ions removed.

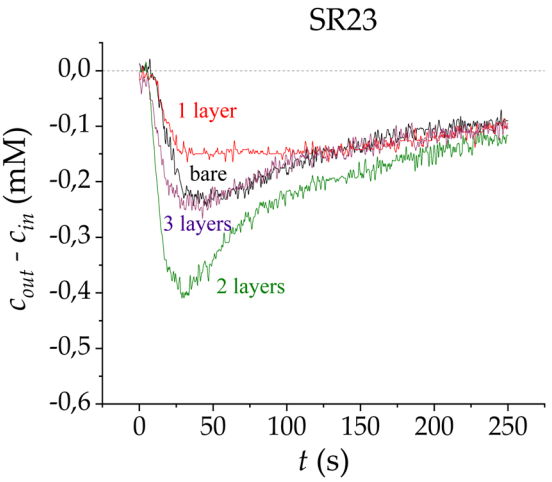

Fig. 3 Ion concentration difference measured at the cell outlet in adsorption stages for bare carbon electrodes (black), and coated carbon electrodes with one (red), two (green) and three (purple) PE layers, using the LbL technique on SR23 carbon electrodes.

The CDI process using SEs has been studied previously,[6,9,15] with promising results over both those obtained with the standard CDI technique and with membrane-assisted CDI. The coating of SR23 with the first layer of polymer (Fig. 3) provokes a slightly lower saline concentration difference compared with that obtained using the bare carbon. The similarities between these curves can be explained by considering that the effectiveness of the coating depends on the polyelectrolyte layer charge density and thickness.

For this reason, the surface composition of the coated carbons has been analyzed by using EDX (Energy Dispersive X-rays) spectroscopy. The sample was prepared *via* lyophilization and transversally cut in order to be able to observe how much the polymer has penetrated into the carbon pores. Fig. 4 shows the carbon sample, as well as the presence of sulfur and sodium ions as indicators for the PSS layer.

As shown in Fig. 4, the first polyelectrolyte coating is not uniform along the entire carbon sample, reducing the performance of the layer in salt adsorption. However, it indeed

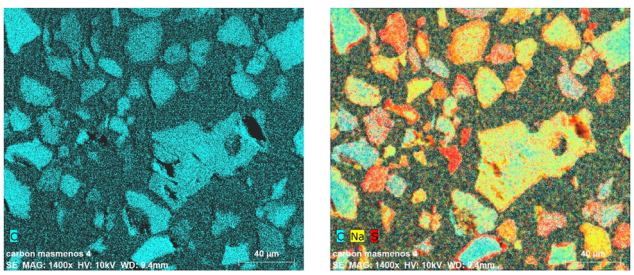

Fig. 4 EDX images of the SR23 carbon coated with a PSS layer. Image colors correspond to carbon (blue), and the specific ions of the polymer: sodium (yellow) and sulfur (red). Left: Only carbon is colored. Right: PSS marked by sodium and sulfur color codes.

improves the efficiency of the process as we will see in Section 3.3. It can be appreciated that not all the carbon is coated and that some of the carbon surface is covered as a whole without penetration of the polyelectrolyte in the inner region of the macropores. This image confirms our assumptions and supports the decision to add another layer with opposite polarity whose adhesion will be favored by the presence of the first layer.

3.1.2. Coating effect: multiple layers. The presence of the second layer gives way to an eye-catching phenomenon. As the charge of the first layer has the same polarity as the electrode that it is deposited on, the second layer polarity is then contrary to the electrode. In this configuration, which we called "opposite polarity" in Fig. 5, the ion adsorption is strongly blocked. We hence checked the effect of switching the polarity of the electrodes, so that the electrode polarity and the sign of the last deposited polymeric layer are identical, a situation that we label "Identical Polarity" in Fig. 5. As observed, ion adsorption is promoted in this configuration, as shown by the notable adsorption cycles; the changes in conductivity measured lead to an enclosed area under the curve which is 4.4 times bigger than the one obtained for the "opposite polarity" configuration.

A third layer was also deposited using the LbL technique, and measurements were made by connecting the electrodes with the same polarity as the charge sign of the last deposited layer. Fig. 3 shows the adsorption stages for the multilayer-electrode configurations, and the electrode polarities are kept equal in sign as their last layers for each measurement. As observed, the addition of the third layer does not produce any improvement over the bare electrodes; this adsorption loss might be due to the similarities this configuration has with respect to the electrodes with only one layer (SE). In contrast, the major improvement in adsorption can be appreciated when coating the electrodes with two layers, with a peak that is almost twice that obtained with bare electrodes.

These results suggest that the first polyelectrolyte layer partially penetrates the macropores, which does not seem to be improving the performance of the system. Nonetheless, although this first polymeric layer was not evenly adhered or dense on the macropores, it acts as a support for the second layer to strongly adhere to the previous one. Therefore, the first coating of the electrodes was not completely efficient but serves as a seed so that the second layer does adhere optimally.

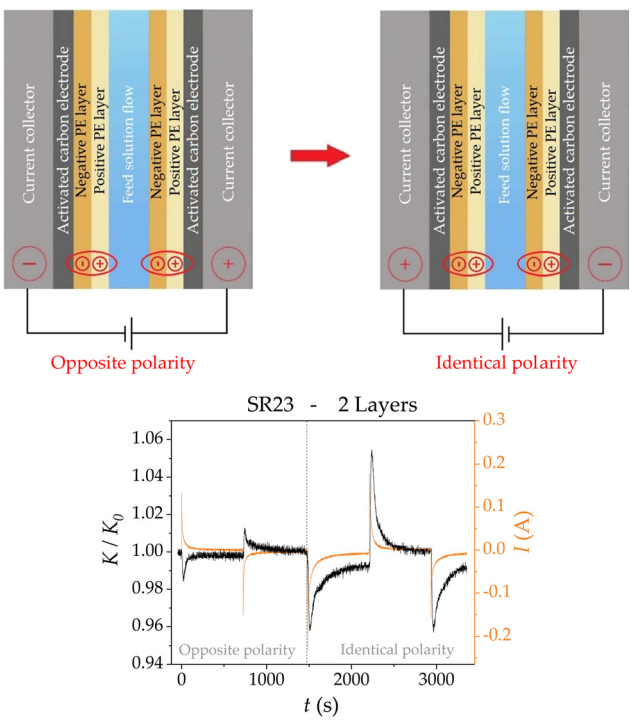

Fig. 5 Top: Scheme of the electrode configuration in "Opposite polarity" (the electrode polarity is opposite to that of the sign of the outer layer; left picture), and the "Identical polarity" (the signs of the electrode and outer layer charges are the same). Bottom: Relative conductivity at the cell outlet (black) and current intensity (orange) measured in the process of charge polarity change.

3.2 YP-80F carbon electrodes

3.2.1 Bare carbon electrodes and soft electrodes: first layer effect. For the YP-80F carbon electrodes, as shown in Fig. 6, we observe a notable improvement in adsorption when using SEs over bare carbon ones, reaching peaks in ion concentration differences that are almost twice those obtained with the initial electrode configuration, and the area under the curve is significantly higher, which will be shown in the calculated salt adsorption capacity.

This positive impact of the first PE layer might be explained because of a better adherence of this first polymeric layer onto the electrode surface, unlike the observations for the previously studied carbon. Intrinsic carbon properties could be the reason for this main difference when coating the electrodes, as the larger specific surface area of this carbon will favour a better adherence being expected for the layer. This matches the data available for both carbons used: the first PE layer seems to be more evenly deposited for the YP-80F carbon, whose specific area, 2271 $m^2 g^{-1}$, is more than twice that of SR23. The macropore/micropore size

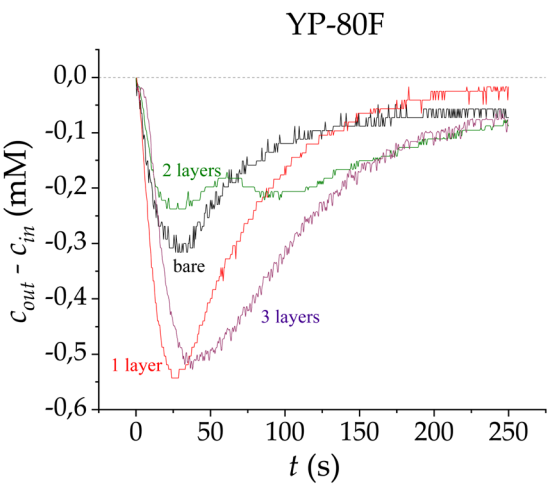

Fig. 6 Ion concentration difference measured at the cell outlet in adsorption stages for bare carbon electrodes (black), and carbon electrodes coated with one (red), two (green) and three (purple) PE layers, using the LbL technique on YP-80F carbon electrodes.

distribution also plays an important role, as smaller micropores (1 nm in the case of YP-80F, and 6–7 nm for SR23) are less accessible for the PE layer to penetrate them, whereas wider macropores are easily lined by the polymer. Our results indicate that the YP-80F carbon surface would seem even and continuous to the polymer coating, favoring its adherence.

3.2.2. Coating effect: multiple layers. In order to obtain the best possible result in each case, every measurement is carried out under the same conditions as the previously studied carbon, that is, keeping each electrode polarity equal in sign to the charge density of the last PE layer deposited. The application of a second layer on the YP-80F carbon electrodes gives way to a completely different behaviour than the one observed in the previously studied carbon: the peak in the adsorption curve turns out to be smaller than that obtained for the one-layer configuration, and so will be the area under the curve (see Fig. 6). As mentioned above, we can suppose that its micropores are open to larger macropores, which would give an explanation for the uniform deposition of the first PE layer on the electrode surface. This gives rise to an improvement in adsorption, but also would allow the second layer to adhere to the previous one with a similar but opposite charge density. Both layers would counteract each other, neither favoring nor blocking (as compared to bare carbon) the global ion flux between the feed solution and the micropores.

The application of a third layer gives way to an adsorption peak that is similar to that corresponding to the one-layer configuration, with a notable increase in the area under the adsorption curve, improving the performance of adsorption.

3.3. Efficiency, salt adsorption and consumed energy

To quantify the performance of each electrode configuration in CDI processes, three main parameters were calculated: the specific adsorption coefficient (SAC), the charge efficiency and the energy per ion consumed in the process.[16]

The specific adsorption coefficient, SAC, expresses the ratio of grams of ions adsorbed per gram of electrode:

$$\mathrm{SAC} = \frac{M_{\mathrm{sal}}}{m_{\mathrm{elect}}} n \tag{2}$$

where M_{sal} is the molar mass of the saline component, m_{elect} is the dry electrode mass, and n is the total number of adsorbed salt moles. This latter parameter was calculated as:

$$n = \int_0^{t_{\mathrm{ads}}} (c_{\mathrm{out}}(t) - c_{\mathrm{in}}) \varphi_{\mathrm{v}} \mathrm{d}t \tag{3}$$

where φ_{v} is the pumping velocity of the solution through the cell, and t_{ads} is the duration time of the adsorption stage.

The charge efficiency of the system, Λ, was calculated as the ratio between the total number of adsorbed salt moles and the charge transferred between the electrodes in the same amount of time. Therefore, when an ion is retired per charge unit deposited on the electrodes, the efficiency will take its maximum value ($\Lambda = 1$).[7,17] Then:

$$\Lambda = F \frac{\int_0^{t_{\mathrm{ads}}} (c_{\mathrm{out}}(t) - c_{\mathrm{in}}) \varphi_{\mathrm{v}} t}{Q} = F \frac{\int_0^{t_{\mathrm{ads}}} (c_{\mathrm{out}}(t) - c_{\mathrm{in}}) \varphi_{\mathrm{v}} \mathrm{d}t}{\int_0^{t_{\mathrm{ads}}} I(t) \mathrm{d}t} \tag{4}$$

where Q is the charge stored during the adsorption stage, $I(t)$ is the instantaneous current at a given time, and F = 96 487 (C mol^{-1}) is the Faraday constant.

The energy consumed per ion removed from the solution in the adsorption stage, E, was calculated as:

$$E = \frac{\int_0^{t_{\mathrm{ads}}} V_{\mathrm{ext}} I(t) \mathrm{d}t}{2 \int_0^{t_{\mathrm{ads}}} (c_{\mathrm{out}}(t) - c_{\mathrm{in}}) \varphi_{\mathrm{v}} \mathrm{d}t} \tag{5}$$

where V_{ext} is the external voltage applied to the cell during the process.

Table 1 Obtained values for the charge efficiency, specific adsorption coefficient (SAC), energy per ion for SR23 carbon electrodes

SR23			
Electrode configuration	Charge efficiency (±0.01)	SAC (mg g^{-1}) (±0.3)	Energy per ion (kT)
Bare	0.55	2.2	42 ± 4
1 Layer	0.57	2.0	41 ± 4
2 Layers	0.87	3.2	27 ± 3
3 Layers	0.70	2.2	34 ± 4

These calculated parameters are shown in Table 1 and graphically displayed in Fig. 7a for SR23 electrodes, and in Table 2 and Fig. 7b for YP-80F electrodes. By comparing to a capacitor, the capacitance C is obtained from exponentially fitting the adsorption-stage current curve, with a characteristic time τ equal to RC, where R is the system resistance. Note that the PE layers (in pairs) barely affect the system resistance, as the differences observed amount to less than 1 Ω, comparable with those of the ion exchange membranes.[18,19]

For SR23 carbon (Fig. 7a), we observe similar behavior between the obtained SAC for bare electrodes and SEs (one layer). However, the calculated charge efficiency is slightly higher in the coated electrode case. This could be explained for a first weak or partial layer attached to the surface of carbon as can be seen in Fig. 4. The use of a second layer gives way to a notable improvement in the amount of adsorbed ions, reaching the maximum value of almost 3.5 mg of NaCl removed from the feed solution for each gram of carbon. This result shows that the second coating is denser than the first one (and probably promoted by the presence of the first layer), in the case of SR23 carbon, increasing the capacity of the cell. The efficiency of the two layer-electrode configuration reaches a remarkable value of almost 0.9. Finally, application of a third polymer layer brings about similar results in capacity to the bare carbon electrodes, but still involves an efficiency improvement over both bare and soft electrodes.

For YP-80F (Fig. 7b) carbon electrodes, and as expected from the adsorption curves, the calculated SAC improves in the cases of one-layer and three-layer configurations, reaching the maximum value with the latter, of around 2.3 mg g^{-1}. The adsorption capacity decline observed in the curve corresponding to

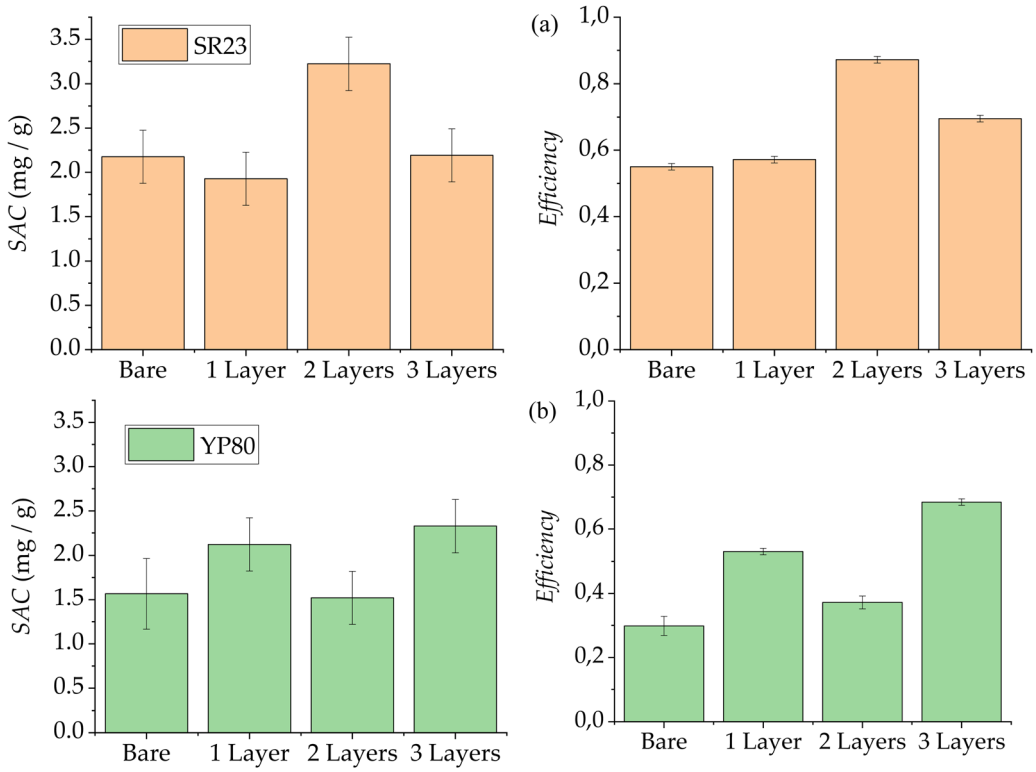

Fig. 7 Quantitative results obtained for SR23 (a, orange bars) and YP-80F (b; green) carbon electrodes using 10 mM NaCl as feed aqueous solutions. Left: Specific adsorption coefficient (SAC). Right: Charge efficiency.

Table 2 Obtained values for the charge efficiency, specific adsorption coefficient (SAC), and energy per ion for YP-80F carbon electrodes

YP-80F			
Electrode configuration	Charge efficiency	SAC (mg g^{-1})	Energy per ion (kT)
Bare	0.30 ± 0.03	1.6 ± 0.4	78 ± 7
1 Layer	0.53 ± 0.01	2.1 ± 0.3	44 ± 4
2 Layers	0.37 ± 0.02	1.5 ± 0.3	63 ± 5
3 Layers	0.68 ± 0.01	2.3 ± 0.3	34 ± 4

two-layer configuration is also exhibited in the SAC, reaching the minimum value: 1.5 mg g^{-1}.

Charge efficiency has a similar behaviour and is inverse to SAC, as the efficiency is higher in the case of YP-80F electrodes with three polymeric layers, with a value of almost 70%. Despite the SAC being minimum for the two-layers configuration, its efficiency value turns out to be slightly higher than the one obtained with bare carbon electrodes. The minimum efficiency value is around 30% for bare carbon showing that, despite having stored a lot of charge, it is not able to remove ions from the solution main stream as will be seen from the theoretical predictions.

As mentioned above and displayed in Fig. 7, although the charge efficiency of the polyelectrolyte-coated electrodes is increased in all the cases shown over that of bare electrodes, SAC is improved or reduced depending on whether the use of multiple layers favours ion transport or if it blocks it, respectively. Therefore, improvements in the adsorption capacity of the system have been quantified and such improvements are found with an even number of polyelectrolyte layers for SR23 carbon electrodes, and an odd number of them for YP-80F ones.

Finally, the consumed energy (see Tables 1 and 2) yields opposite trends than the efficiency, as expected: the larger the energy spent, the lower the efficiency of the system. This relationship holds as the minimum energy spent takes a value of around 27 k_BT per ion in the two layers-electrode configurations for the SR23 carbon, and a value of around 34 k_BT for the three layers-electrodes in the case of YP-80F.

4. Theoretical predictions

The interface between a coated porous electrode and ionic solution can be modeled assuming that the polymeric layer covers the macropore walls, affecting only the ion transport between these and the micropores (Fig. 8). We consider that the polymer layer is a region with a certain charge distributed in a volumetric region that extends from the macropore surface and it is permeable to the ions.

Two regions have to be considered to determine the electric potential profile and the ion distribution by solving Poisson's equation, namely, the external region, where charge is given by the ion concentration; and the polymer shell, where the polymer charge density, ρ_{pol}, also has to be taken into account.

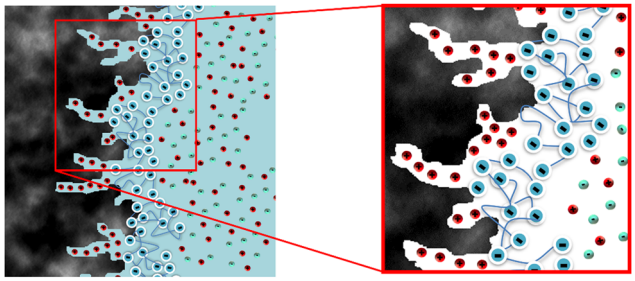

Fig. 8 Scheme of the positioning of the PE layer on the electrode surface. The layer coats the macropore walls, regulating the ion flux to the micropores.

This is shown in the following equation:

$$\begin{cases} \nabla^2\psi = -\dfrac{1}{\varepsilon\varepsilon_0}\sum_{j=1}^{N} z_j F c_j & \text{outside the PE layer} \\ \nabla^2\psi = -\dfrac{1}{\varepsilon\varepsilon_0}\sum_{j=1}^{N} z_j F c_j - \dfrac{1}{\varepsilon\varepsilon_0}\rho_{\text{pol}} & \text{inside the PE layer} \end{cases} \quad (6)$$

where F is the Faraday constant, Ψ is the electric potential, c_j (mol m^{-3} or mM) is the concentration of the j-th ionic species in the solution, z_j is its corresponding valence, and $\varepsilon\varepsilon_0$ is the relative permitivity in the outer region. The ion concentration is given by the Boltzmann distribution:

$$c_j = c_{j_0}\exp\left(-\frac{z_j e\psi}{k_B T}\right) \quad (7)$$

where the initial concentration, far from the charged surface, of ion species j in the solution feed is denoted by c_{j_0}.

The model proposed for a single PE layer can be extended to several layers by modifying the set of equations (eqn (6)) and their corresponding boundary conditions (the electric field satisfies the Gauss law on the solid surface and vanishes far from this; the electric potential is continuous between successive polyelectrolyte layers) in order to predict the ion distribution around the solid surface, and thus deduce the impact of the multiple coating.

The time response of the ion concentration at the cell outlet can be predicted. For this, a 1-D model is used (as described by Tang *et al.*[20] and Biesheuvel *et al.*[21] and modified in ref. 6 and 9) which only considers one spatial variable along the cell for a coated electrode with one polymer layer. In this model, the cell is divided into i subcells ($i = 1, \ldots, M$; being M the total number of subcells) perpendicular to the solution flow so that, for each ionic species j present in the solution, each subcell has an ion concentration $c_{j,i}$. This subcell concentration suffers changes due to the ion transport from the previous cell ($i - 1$), as well as the ion flux from the macropores to the micropores, and *vice versa*, $J_{j,i,\text{mA}\to\text{mi}}$:

$$\left(L_{\text{sp}} + 2L_e p_{\text{mA}}\right)\frac{\mathrm{d}c_{j,i}}{\mathrm{d}t} = -J_{j,i,\text{mA}\to\text{mi}} + \frac{\varphi_v}{A_{\text{sub}}}\left(c_{j,i-1} - c_{j,i}\right) \quad (8)$$

where L_{sp} is the spacer channel length, L_e is the thickness of the electrodes, p_{mA} is the macroporosity, and A_{sub} is the projected area of the electrodes for each subcell.

At the same time, the charge density of the micropores, $\rho_{\text{mi},i}$, in contact with the macropores in the i-th subcell varies according to each ion species flux contribution:

$$-L_e\frac{\mathrm{d}}{\mathrm{d}t}\left(p_{\text{mi}}\rho_{\text{mi},i}\right) = \sum_{j=1}^{N} z_j J_{j,i,\text{mA}\to\text{mi}} \quad (9)$$

where p_{mi} is the microporosity. The ion flux is given by the Nernst–Planck equation, assuming that there is only an electrostatic contribution, and no saline concentration gradient along the macropores (direction perpendicular to the feed solution flow):[22–25]

$$J_{j,i,\text{mA}\to\text{mi}} = z_j D_j c_{j,i}^{\text{SE}} L_{\text{eff}}^{-1}\Delta\phi_{\text{tr},i} \quad (10)$$

where D_j is the diffusion coefficient of each ion species, L_{eff} is an effective length which determines the mean electric field between the electrodes, $\Delta\phi_{\text{tr},i}$ is the electric potential difference which generates ion transport, and $c_{j,i}^{\text{SE}}$ is the ion concentration inside the polymer layer, which is also the one found at the entrance of the micropores, and it is calculated by solving eqn (6), as described above.

The electric potential difference is calculated as the difference between the external voltage applied to the cell, V_{ext}, and the potential drop observed along the EDL (including Stern and diffuse layers). Then:

$$\Delta\phi_{\text{tr},i} = V_{\text{ext}}/V_T - 2\left|\Delta\psi_{\text{Stern}} + \Delta\psi_d\right| \quad (11)$$

where $V_T = k_B T/e$ is the thermal voltage. Dimensionless potential difference values of the Stern and diffuse layers, $\Delta\Psi_{\text{Stern}}$ and $\Delta\Psi_d$, respectively, are calculated by taking the modified Donnan model (mD) into account.[7,26–28] This model considers a constant Donnan equilibrium for the electric potential inside the micropore, since the Debye length is significantly larger than the micropore diameter when working with typical CDI salt concentrations. For the monovalent electrolyte case ($c_{j,i} = c_i$):

$$\begin{aligned} \Delta\psi_{\text{Stern}} &= -\frac{\rho_{\text{mi},i}F}{C_{\text{St}}V_T} \\ \Delta\psi_{d,i} &= \sinh^{-1}\left(-\frac{\rho_{\text{mi},i}}{2c_i}\right) \end{aligned} \quad (12)$$

where C_{St} is the Stern layer capacitance (per unit volume). As a boundary condition, $\rho_{\text{mi},i}$ must be 0 at $t = 0$. In addition, $c_{j,i} = c_{j_0}$ at the initial time.

This model must be modified for the multilayer case. The ion transport and the EDL screening can be modeled as the charge stage of an RC circuit. Then, the addition of multiple layers is equivalent to the arrangement of resistors in series, as the current intensity will take the same value through the different layers. For the single-layer case, if we compare eqn (10) to Ohm's law:

$$J_{j,i,\text{mA}\to\text{mi}} = \frac{\Delta\phi_{\text{tr},i}}{A_{\text{sub}}R_j} \quad (13)$$

the resistance R_j of the monolayer system can be easily identified:

$$R_j = \frac{L_{\text{eff}}}{A_{\text{sub}} z_j D_j c_{j,i}^{\text{SE}}} \tag{14}$$

Considering a total number of layers, N_{layers}, the equivalent resistance would be the sum of the individual resistances of each layer, $R_{j,k}$ ($k = 1, \ldots, N_{\text{layers}}$). Therefore, the ion fluxes and resistances will be written as follows:

$$\begin{aligned} J_{j,i,\text{mA}\rightarrow\text{mi}} &= \frac{\Delta\phi_{\text{tr},i}}{A_{\text{sub}} \sum_{k=1}^{N_{\text{layers}}} R_{j,k}} \\ R_{j,k} &= \frac{L_{\text{eff}}}{A_{\text{sub}} z_j D_j c_{j,i}^{\text{SE}_k}} \end{aligned} \tag{15}$$

The electric potential difference which generates ion transport is also affected by the potential difference of each polymer layer, $\Delta\Psi_k$:

$$\Delta\phi_{\text{tr},i} = V_{\text{ext}}/V_{\text{T}} - 2|\Delta\psi_{\text{Stern}} + \Delta\psi_{\text{d}}| - \sum_{k=1}^{N_{\text{layers}}} \Delta\psi_{k,i} \tag{16}$$

It is supposed that there is no ion accumulation between layers. Using the constraint that the ion flux through each individual layer must be equal to the one calculated globally, $\Delta\Psi_{k,i}$ can be calculated separately from $R_{j,k}$:

$$\Delta\Psi_{k,i} = J_{j,i,\text{mA}\rightarrow\text{mi}} R_{j,k} \tag{17}$$

As the electrodes coated with one and two polymeric layers seem to offer the most relevant results, the theoretical predictions have been analyzed for these mentioned cases. The previous equations are solved using the BVP4C numeric routine from Matlab®.

Fig. 9a and b show the ionic concentration profile near a positively charged surface, coated with two polymeric layers of alternate charge polarities, obtained by solving the set of eqn (6). In Fig. 9 we can observe the formation of the EDL next to the surface. In cases (a) and (b) there is a coating of two polymer layers, in such a way that the ionic concentration increases or decreases with respect to that of the medium, 10 mM, depending on the ion polarity with respect to the polymer layer charge. Alternatively, Fig. 9c, without polymer coatings, shows that the EDL is formed with an excess of counterions and defect of coions from the medium (10 mM). The effect of the PE layer is to produce an excess (defect) of ionic concentration that brings about an increase (reduction) in the flow of that type of ions, favoring (blocking) their adsorption (desorption). This enhances the efficiency of the process because the entry of counterions is promoted to compensate the surface electric charge, while the exit of coions is prevented.

To simulate the case of the SR23 carbon electrode, based on EDX images (Fig. 9a and 10a) and the behaviour of the experimental results, the fitted value of the first layer's charge

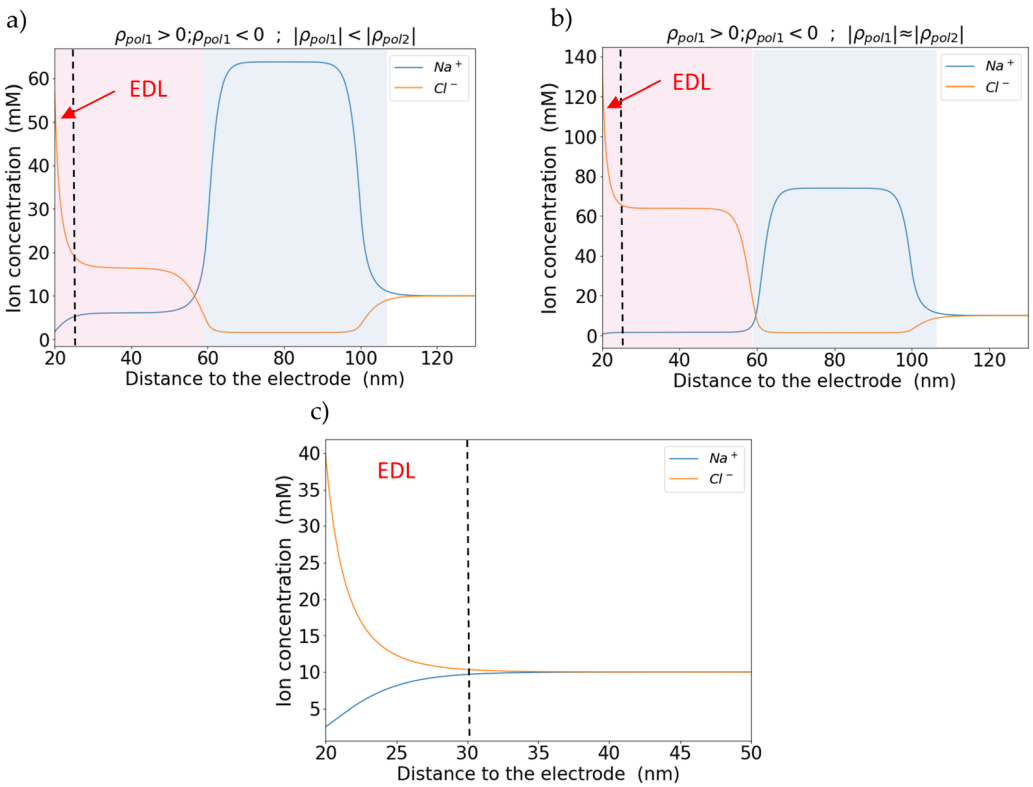

Fig. 9 Theoretical curves for sodium (blue) and chloride (orange) concentration as a function of the distance to a positively charged electrode coated with two PE layers. The feed solution is 10 mM NaCl. (a) $\rho_{\text{pol}1} = 1 \times 10^6$ (C m^{-3}); $\rho_{\text{pol}2} = -6 \times 10^6$ (C m^{-3}). (b) $\rho_{\text{pol}1} = 6 \times 10^6$ (C m^{-3}); $\rho_{\text{pol}2} = -7 \times 10^6$ (C m^{-3}). (c) Bare electrode for comparison.

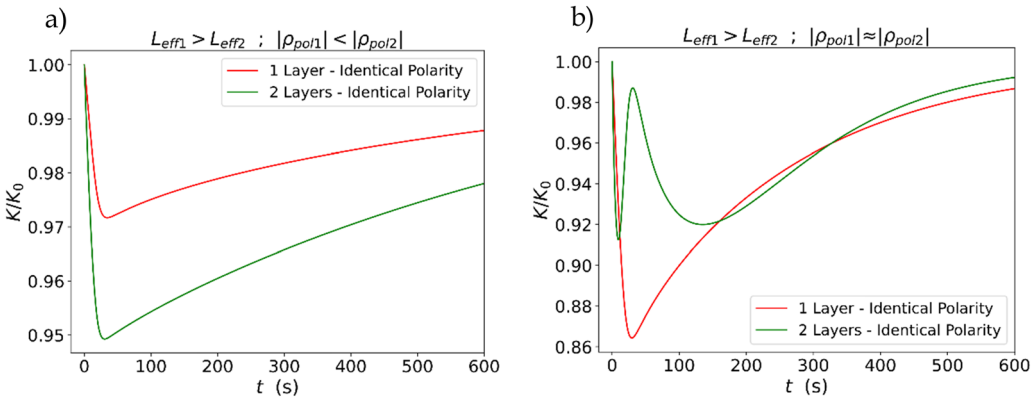

Fig. 10 Relative conductivity of an adsorption stage calculated from theoretical simulations for one (red) and two (green) polyelectrolyte layers coating the electrode. In all cases, identical polarity between the electrode and the outermost polymer layer change. (a) The SR23 carbon case by fitting a lower charge density to the first PE layer. (b) The YP-80F case, fitting approximately the same charge density between two layers.

density was lower than that of the second layer. Since the charge density of the second layer is higher in this case, the counterion (Na^+) transport is highly favoured while the coion (Cl^-) transport is strongly blocked.

Using these ionic concentration distributions, eqn (8)–(17) can be solved to obtain the theoretical predictions of the dynamic response of the SR23 carbon electrode for one and two polymeric layers in the adsorption step. In the latter case, the electrode charge polarity is identical to that of the external polymer coating (Fig. 5). The predicted relative conductivity (Fig. 10a) has the same behaviour as the experimental results (Fig. 3), regarding the increase in salt adsorption with the addition of the second layer. The model predicts that adding a second PE layer on top of the first one of lower charge density and different polarity results in a higher adsorption and efficiency (Table 1) than the weakly deposited first layer.

To simulate the YP-80F carbon electrode case, the charge densities of both layers have been assumed to be similar but with opposite sign. Fig. 10b shows the ionic concentration profile, with their transport favoured in one of the layers (where it acts as a counterion) and strongly blocked in the other one (acting as a coion). As a result, the combination of the two layers with identical charge densities give way to an antagonistic effect, which leads to a lower adsorption predicted at the cell outlet. Note that the theoretical prediction using this assumption agrees very well with the experimental results (Fig. 6), showing even a desorptive-like ''hump'' behaviour (Fig. 10b).

5. Conclusions

Capacitive deionization (CDI) is based on the properties of the electrical double layer of porous electrodes. Properties such as their overall porosity and their micro/macro-porous distribution are fundamental in determining the storage capacity for ion adsorption when applying a potential difference between two electrodes in contact with a salt solution. The functionalization of the electrodes using polyelectrolyte coatings opens a new way to improve the performance of the method and its capability to implement, in the near future, ion selective adsorption.[29] For both aims, the use of successive layers of alternating charge signs to reinforce the adsorption or to set one of the layers to be selective to one of the ionic species is found to be very interesting. In this work, we found that such layers improve the adsorption and efficiency, although the results depend on the internal structures of the porous structure of the activated carbon.

Surface modification has been studied for two different activated carbon electrodes, denominated SR23 and YP-80F, coating them with up to three PE layers using the Layer-by-Layer (LbL) technique to analyze the impact of the coating and its dependence on carbon properties such as porosity and specific surface.

SR23 carbon electrodes present a weak adherence of the first PE layer, although this favours the coating of the following layer, with an opposite charge density polarity, acting as a support. This second layer provides the highest ion adsorption and efficiency values, reaching respectively 3.2 mg g^{-1} and 87% of efficiency, to be compared to 2.2 mg g^{-1} and 55% for bare SR23. It is highlighted that these results have been achieved when the polarity of the surface charge of the electrode coincides with that of the outer layer.

On the other hand, coating with an odd number of PE layers seems to be more consistent on the YP-80F carbon electrodes, and the addition of even layers blocks the ion transport. The reason for this lies on the similar uniformity of the first and second coatings and their opposite charge polarity, creating an antagonistic effect on ion transport (neither favoured nor blocked) due to charge compensation. For these carbon electrodes, the three-layer configuration provides the highest ion adsorption and efficiency values, reaching 2.3 mg g^{-1} and 68%, respectively. These figures are 1.6 mg g^{-1} and 30% for uncoated YP80.

A theoretical model for the multiple-layer configurations has been presented, which determines the temporal evolution of each ion species concentration while considering ion transport from the feed solution to the micropores. It is notable to

mention the qualitative agreement between the theoretical predictions of this model and the experimental results if the proposed hypothesis about the density of the PE layers is considered.

Conflicts of interest

There are no conflicts of interest to declare.

Acknowledgements

Financial support of this investigation by FEDER/Junta de Andalucía-Consejería de Transformación Económica, Industria, Conocimiento y Universidades, Spain (Grant No. P20_00233) and Consejería de Conocimiento, Investigación y Universidad, Junta de Andalucía, Spain (Grant No. A-FQM-492-UGR20) is gratefully acknowledged. Thanks are also due for the grant TED2021-131855B-I00/AEI/10.13039/501100011033/Unión Europea Next-GenerationEU/PRTR.

References

1 J. W. Blair and G. W. Murphy, *Advances in Chemistry Series Number 27*, American Chemical Society, Washington, DC, 1960.
2 *Lewabrane, Principles of Reverse Osmosis Membrane Separation*, Lanxess Deutschland GmbH, Köln, Germany, 2013.
3 A. Delgado, *Interfacial electrokinetics and electrophoresis*, Elsevier, New York, 2002.
4 A. V. Delgado, M. L. Jiménez, G. R. Iglesias and S. Ahualli, *Curr. Opin. Colloid Interface Sci.*, 2019, **44**, 72–84.
5 A. D. Khawaji, I. K. Kutubkhanah and J. Wie, *Desalination*, 2008, **221**, 47–69.
6 S. Ahualli, G. Iglesias, M. M. Fernández, M. L. Jiménez and A. V. Delgado, *Environ. Sci. Technol.*, 2017, **51**, 5326–5333.
7 S. Porada, R. Zhao, A. Van Der Wal, V. Presser and P. M. Biesheuvel, *Progress in Materials Science*, 2013, **58**(8), 1388–1442.
8 R. Zhao, *Theory and operation of capacitive deionization systems*, Wageningen University and Research, Netherlands, 2013.
9 S. Ahualli, S. Orozco-Barrera, M. M. Fernández, A. V. Delgado and G. R. Iglesias, *Polymers*, 2019, **11**(10), 1556.
10 G. Decher, *Science*, 1997, **277**, 1232–1237.
11 J. J. Richardson, M. Björnmalm and F. Caruso, *Science*, 2015, **348**, 6233.
12 J. J. Richardson, J. Cui, M. Björnmalm, J. A. Braunger, H. Ejima and F. Caruso, *Chem. Rev.*, 2016, **116**(23), 14828–14867.
13 A. V. Delgado, S. Ahualli, M. M. Fernández, M. A. González, G. R. Iglesias, J. F. Vivo-Vilches and M. L. Jiménez, *Environ. Chem.*, 2017, **14**(5), 279–287.
14 S. Nadakatti, M. Tendulkar and M. Kadam, *Desalination*, 2011, **268**(1–3), 182–188.
15 S. Ahualli, M. L. Jiménez, M. M. Fernández, G. Iglesias, D. Brogioli and A. V. Delgado, *Phys. Chem. Chem. Phys.*, 2014, **16**, 25241–25246.
16 M. E. Suss, S. Porada, X. Sun, P. M. Biesheuvel, J. Yoon and V. Presser, *Energy Environ. Sci.*, 2015, **8**(8), 2296–2319.
17 R. Zhao, P. M. Biesheuvel, H. Miedema, H. Bruning and A. Van der Wal, *J. Phys. Chem. Lett.*, 2009, **1**(1), 205–210.
18 P. Długołęcki, P. Ogonowski, S. J. Metz, M. Saakes, K. Nijmeijer and M. Wessling, *J. Membr. Sci.*, 2010, **349**(1–2), 369–379.
19 J. Chang, K. Tang, H. Cao, Z. Zhao, C. Su, Y. Li, F. Duan and Y. Sheng, *Sep. Purif. Technol.*, 2018, **207**, 387–395.
20 W. Tang, P. Kovalsky, B. Cao, D. He and T. D. Waite, *Environ. Sci. Technol.*, 2016, **50**(19), 10570–10579.
21 P. M. Biesheuvel, B. van Limpt and A. van der Wal, *J. Phys. Chem. C*, 2009, **113**(14), 5636–5640.
22 P. M. Biesheuvel and A. van der Wal, *J. Membr. Sci.*, 2010, **346**(2), 256–262.
23 T. Kim, J. E. Dykstra, S. Porada, A. van der Wal, J. Yoon and P. M. Biesheuvel, *J. Colloid Interface Sci.*, 2015, **446**, 317–326.
24 S. Porada, L. Borchardt, M. Oschatz, M. Bryjak, J. S. Atchison, K. J. Keesman, S. Kaskel, P. M. Biesheuvel and V. Presser, *Energy Environ. Sci.*, 2013, **6**(12), 3700–3712.
25 R. Zhao, M. van Soestbergen, H. H. M. Rijnaarts, A. van der Wal, M. Z. Bazant and P. M. Biesheuvel, *J. Colloid Interface Sci.*, 2012, **384**, 38–44.
26 B. Kastening and M. Heins, *Electrochim. Acta*, 2005, **50**(12), 2487–2498.
27 W. Tang, P. Kovalsky, D. He and T. D. Waite, *Water Res.*, 2015, **84**, 342–349.
28 A. Hemmatifar, M. Stadermann and J. G. Santiago, *J. Phys. Chem. C*, 2015, **119**(44), 24681–24694.
29 M. E. Suss, *J. Electrochem. Soc.*, 2017, **164**(9), E270–E275.